NOTES AND CORRESPONDENCE

A Comparison of Climate Prediction and Simulation over the Tropical Pacific

VASUBANDHU MISRA, L. MARX, M. FENNESSY, B. KIRTMAN, AND J. L. KINTER III

Center for Ocean–Land–Atmosphere Studies, Institute of Global Environment and Society, Inc., Calverton, Maryland

(Manuscript received 8 March 2007, in final form 24 September 2007)

ABSTRACT

This study compares an ensemble of seasonal hindcasts with a multidecadal integration from the same global coupled climate model over the tropical Pacific Ocean. It is shown that the annual mean state of the SST and its variability are different over the tropical Pacific Ocean in the two operating modes of the model.

These differences are symptoms of an inherent difference in the physics of coupled air–sea interactions and upper ocean variability. It is argued that in the presence of large coupled model errors and in the absence of coupled data assimilation, the competing and at times additive influence of the initialization and model errors can change the behavior of the air–sea interaction physics and upper ocean dynamics.

1. Introduction

In this note we investigate the differences between a set of retrospective seasonal predictions and a long-term (multidecadal) simulation, both made with an identical coupled climate model. The motivation is twofold. One is of practical significance in that coupled model development could be accelerated if the changes made to a coupled model could be tested with short ensembles of integrations, the results of which are similar to those obtained with a multidecadal run. The other motivation is to understand how the imbalance in the initial state obtained from ocean data assimilation leads to an "initialization shock": the rapid adjustment of the coupled model toward its own preferred modes of variability. In a related atmospheric general circulation model (AGCM) study forced with observed SST, Misra (2004) showed that there were significant differences between short-term (seasonal) retrospective predictions and long-term (multidecadal) simulations, due to model bias. In this study we focus on the equatorial Pacific because of its robust ENSO variability, which is a manifestation of strong coupled air–sea interactions (Philander 1983).

Corresponding author address: Vasubandhu Misra, Center for Ocean–Land–Atmosphere Studies, Institute of Global Environment and Society, Inc., 4041 Powder Mill Road, Suite 302, Calverton, MD 20705.
E-mail: misra@cola.iges.org

DOI: 10.1175/2008JCLI1932.1

The specific questions addressed here are the following:

1) How does the mean coupled state in the tropical Pacific differ between the seasonal hindcasts and multidecadal integrations?
2) How does the ENSO variability in the tropical Pacific vary between the seasonal hindcasts and multidecadal integrations?
3) What are the ramifications of these differences regarding model development and prediction of ENSO variability?

In the following section a brief description of the model is given. This is followed by the description of the design of experiments in section 3. In section 4, results are presented, and concluding remarks comprise section 5.

2. Model description

The recently developed Center for Ocean–Land–Atmosphere Studies (COLA) coupled climate model (Misra et al. 2007) is used in this study. The AGCM is used at a spectral resolution of T62 (≈200-km grid resolution) with 28 sigma [$=(p/p_s)$] levels. A brief outline of the AGCM is provided in Table 1. [The readers are referred to Misra et al. (2007) for a detailed description of the AGCM.] This AGCM is coupled to the modular ocean model, version 3.0 (MOM3; Pacanowski and

TABLE 1. The outline of the COLA AGCM used in this study.

Process	V3.2
Advection	Dynamical core (Kiehl et al. 1998); dependent variables are spectrally treated, except for moisture, which is advected by a semi-Lagrangian scheme
Deep convection	Relaxed Arakawa–Schubert scheme (Bacmeister et al. 2000)
Longwave radiation	Collins et al. (2002)
Boundary layer	nonlocal (Hong and Pan 1996)
Land surface process	Xue et al. (1991, 1996); Dirmeyer and Zeng (1999)
Shallow convection	Tiedtke (1984)
Shortwave radiation	Briegleb (1992)
Diagnostic cloud fraction and optical properties	Kiehl et al. (1998)

Griffies 1998). MOM3 has a uniform zonal resolution of 1.5° while the meridional resolution is 0.5° between 10°S and 10°N, gradually increasing to 1.5° at 30°N and 30°S and fixed at 1.5° in the extratropics.

3. Design of experiments

There are 10 ensemble members generated for four different years for the seasonal hindcast integrations (hereafter retrospective predictions), totaling to 40 seasonal retrospective predictions. The 10 ensemble members for a given year in the retrospective prediction runs are generated by varying the initial conditions of the atmosphere while keeping the ocean initial state identical. The 10 atmospheric initial conditions for a given year were obtained by resetting the initial date of the atmospheric restart files after integrating the AGCM for a week from National Centers for Environmental Prediction (NCEP) reanalysis (Kalnay et al. 1996) with time-invarying SST borrowed from observations [extended reconstructed SST, version 2 (ERSST2); Smith and Reynolds (2003)] 7 days prior to the start of the coupled integration. This methodology has been successfully implemented in earlier studies to generate synoptically independent initial conditions of the atmosphere (Kirtman et al. 2001). The land surface initial conditions are identical for all 10 ensemble members in a given year. They are obtained from an offline land data assimilation (Dirmeyer and Tan 2001).

The ocean initial conditions for the retrospective predictions were taken from an ocean data assimilation (ODA; Rosati et al. 1997). The ODA ocean initial states were generated from a higher-resolution ocean model than that used in the ocean component of the coupled model used in this study, with identical physics

TABLE 2. The validation period of the observed datasets.

Variable	Source	Period used for validation
SST	ERSST2 (Smith and Reynolds 2003)	1966–2005
Latent heat flux	GSSTF2 (Chou et al. 2003)	1989–2000
Thermocline depth	ODA (Rosati et al. 1997)	1980–98

and parameter settings. For the coupled experiments of this study, we have interpolated the ocean initial states to the grid resolution of the ocean model used in the coupled model. The initial dates of the retrospective coupled prediction cases were initialized on 0000 UTC 1 December 1982, 1988, 1997, and 1998. The choice of initialization time of these retrospective prediction runs is deliberate to predict some of the strongest ENSO events in recent decades. Furthermore, coupled modeling studies have shown that prediction skills are relatively higher when coupled models are initialized in the boreal winter (Latif et al. 1998; Saha et al. 2006; Jin et al. 2008). The retrospective predictions were all run for 1 yr, thereby in total generating 40 model integration years (=10 ensemble members × 1 yr of integration × 4 cases).

Simultaneously, a multidecadal integration (hereafter simulation) was made with the same coupled model. The ocean initial state for this integration was taken from an ocean restart file of a previous coupled integration (Misra et al. 2007) run for a period of 70 yr with the same coupled model. The atmospheric initial condition was taken from one of the initial conditions of the retrospective predictions. The simulation was made for 60 yr, and the last 40 yr of the run are analyzed for this study.

4. Results

The results from the coupled model simulations are compared with the ERSST2 at 2.0° latitude/longitude horizontal grid resolution, the ODA for subsurface ocean temperatures, and surface latent heat fluxes from version 2 of the Goddard satellite-based sea surface turbulence fluxes (GSSTF2; Chou et al. 2003), available on a 1° × 1° grid. In Table 2 we indicate the period over which these observed datasets are compared to the coupled simulations. It should be noted that the GSSTF2 fluxes are a derived quantity using a bulk aerodynamic algorithm on 10-m wind speed and specific humidity retrieved from Special Sensor Microwave Imager (SSM/I), and 2-m air temperature and SST from NCEP–National Center for Atmospheric Research (NCAR) reanalysis (Kalnay et al. 1996). Comparison of

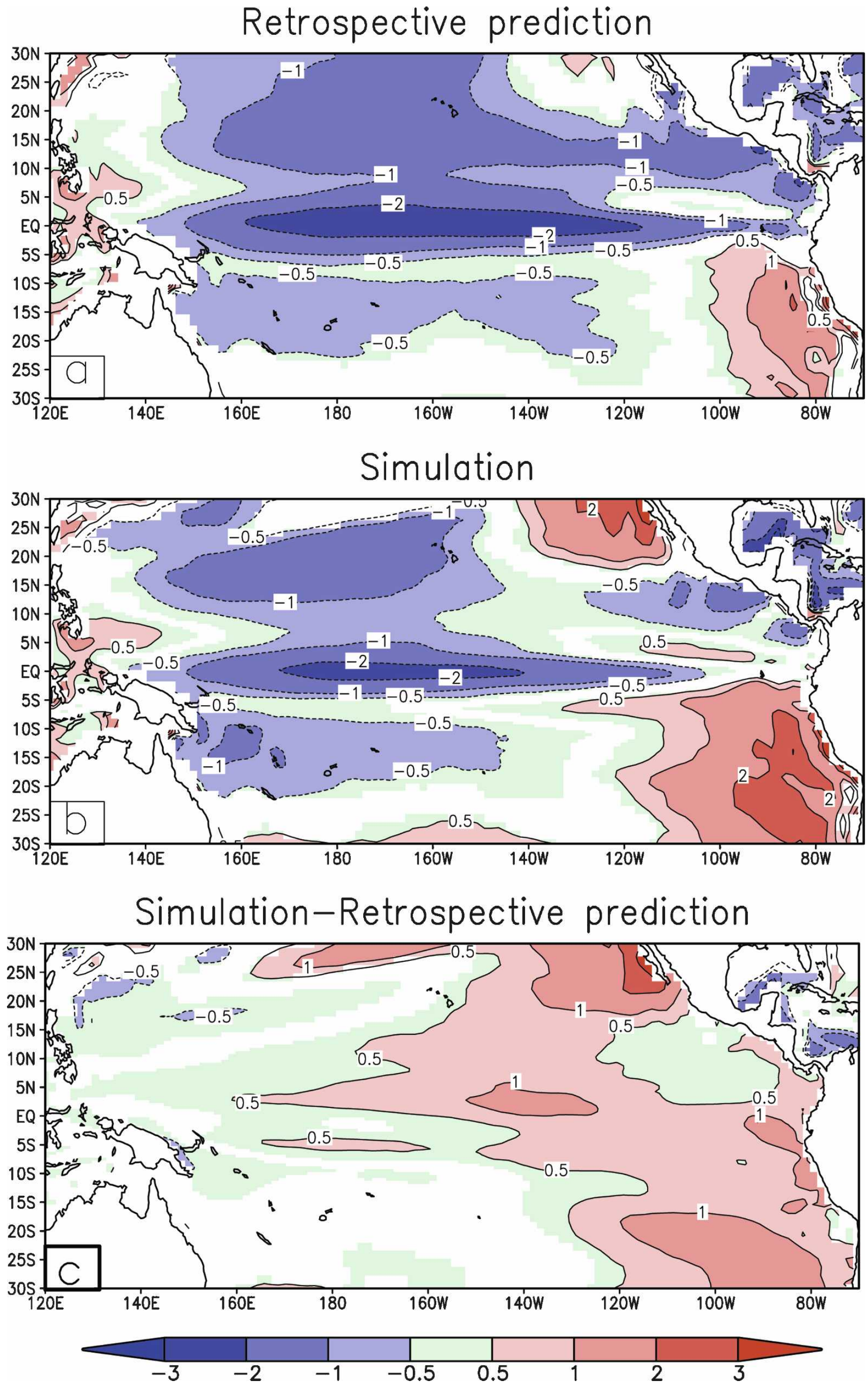

FIG. 1. Climatological annual mean errors of SST from (a) retrospective prediction and (b) simulation runs of the coupled model. (c) The difference in the annual mean climatology of SST between the simulation and the retrospective predictions. The significant values at 90% confidence interval according to a Student's *t* test are shaded in (c).

this flux product with fluxes from 10 other field experiments suggests that GSSTF2 fluxes are reasonable (Chou et al. 2003). The observational period used for model verification is based on either what is available or the latest 40 yr available, unless mentioned otherwise. It should also be noted that the climatology of the retrospective coupled prediction integrations is based on the mean of all 40 cases.

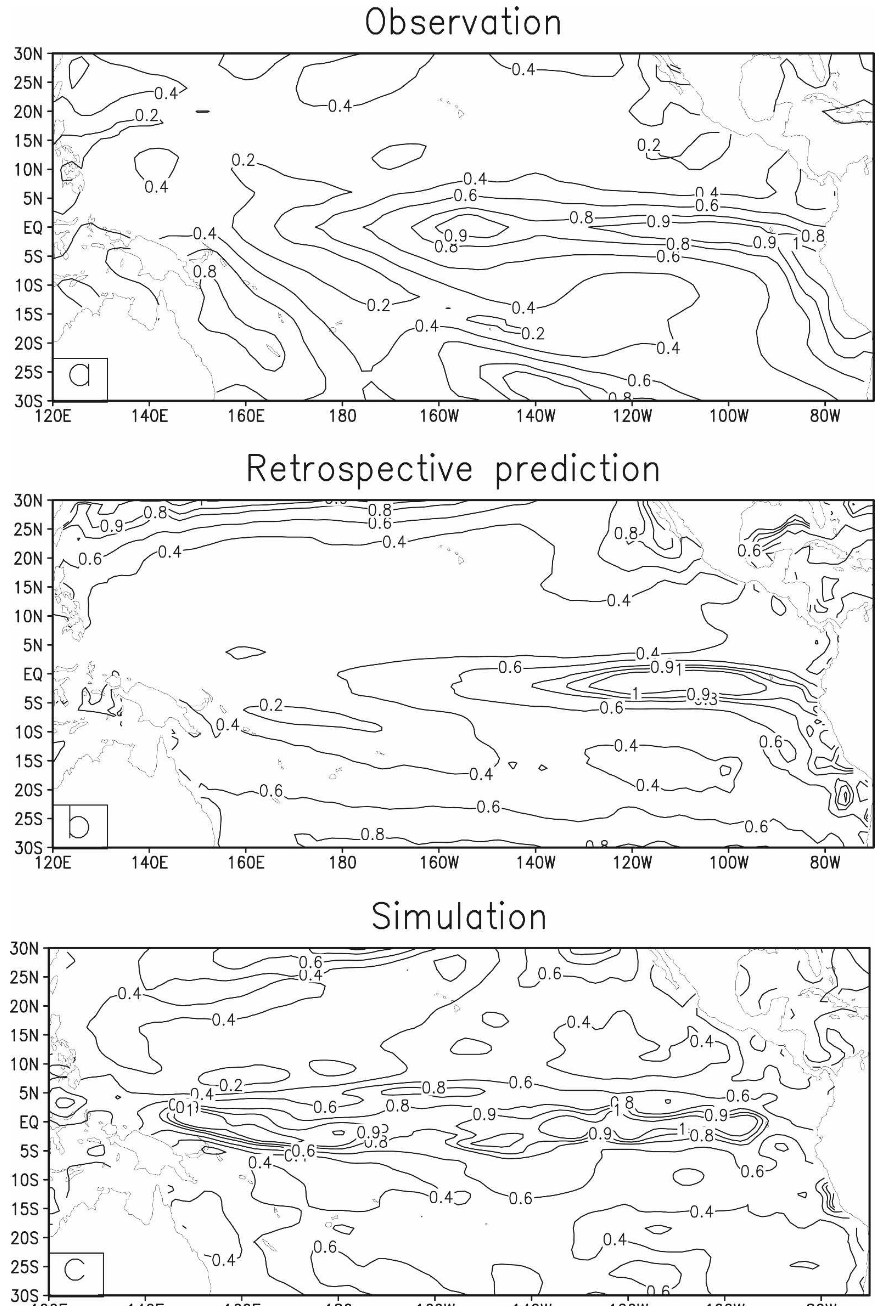

FIG. 2. The std dev of the monthly mean SST from (a) observations, (b) retrospective prediction, and (c) simulation.

a. Differences in annual mean errors

In Fig. 1 we show the annual mean 40-yr climatological errors of SST from the retrospective prediction and simulation experiments. The cold equatorial Pacific bias is more severe by 0.5°–1°C in the retrospective prediction runs compared to that in the simulation over the equatorial Pacific Ocean. However, the errors in the retrospective prediction runs over the stratus deck region in the southeastern Pacific (off the coast of Chile and Peru) are less than those in the simulation.

b. Differences in SST variability

The standard deviation of SST from observations, retrospective prediction, and simulation runs is shown

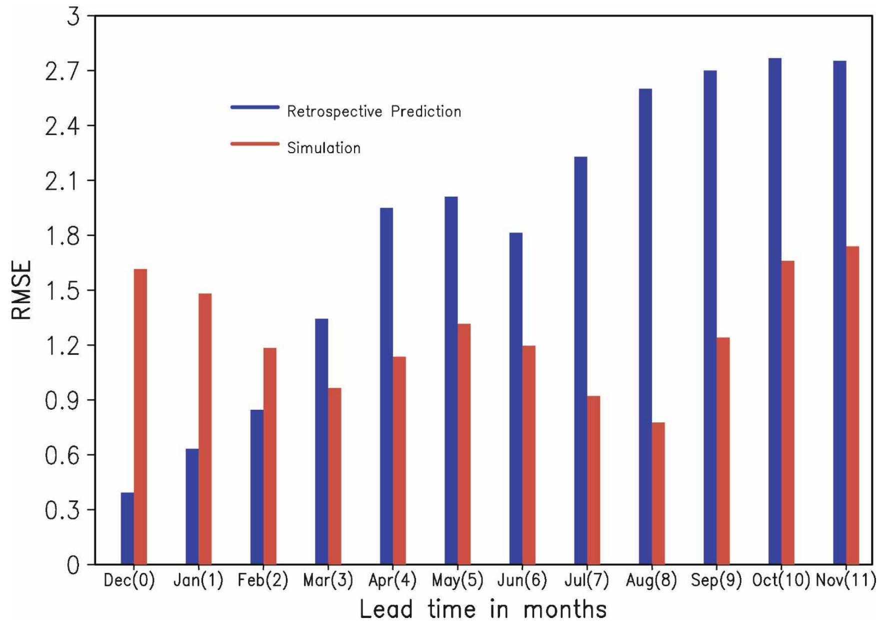

FIG. 3. The RMSE of the retrospective prediction as a function of lead time, and simulation as a function of calendar month.

in Fig. 2. The retrospective prediction has a more realistic SST variability in the equatorial Pacific region than does the simulation. The simulation erroneously has much higher variability in the western Pacific Ocean, suggesting that the coupled model "ENSO mode" is significantly different from nature. Furthermore, the simulation exhibits far less variability along the eastern boundary of the tropical Pacific off the coast of Peru than the retrospective predictions or the observations. These model errors in the simulation are reminiscent of those seen in many other state-of-the-art coupled climate models.

c. Drift as a function of time

In Fig. 3 the root-mean-square errors (RMSEs) of the retrospective predictions (simulation) as a function of lead time (calendar month) over the Niño-3 region are shown. As expected, the RMSEs increase in the retrospective predictions as the lead time increases in a linear fashion. On the other hand, the simulation indicates that the largest RMSEs over the Niño-3 region are in the boreal fall and winter. Obviously, the contrasting behavior of the COLA model in terms of this metric between the retrospective predictions and simulation is a result of the difference in the role of initialization: in the latter, the drift is largely due to model errors, while in the former it is a combination of model and initialization errors.

In Fig. 4 we compare the evolution of the Niño-3 SST anomalies in each year of the retrospective prediction with the corresponding observations. It is noted that for consistency the observed anomalies in this figure are computed from the mean of the 4 yr shown. The ensemble mean over the 10 ensemble members of the retrospective prediction shows a reasonable prediction of both the warm and the cold ENSO events at all lead times. The initial Niño-3 SST anomalies in all 4 yr tend to damp out over the 12-month period of the model integration consistent with the observations.

d. Differences in local air–sea interaction

Wallace et al. (1990), Cayan (1992), and Wu et al. (2006) among many others, have demonstrated that the diagnosis of air–sea interaction is best accomplished by comparing the relationships of atmospheric fluxes with SST and SST tendency. For example, a large positive correlation between latent heat flux and SST may indicate that SST is forcing the atmosphere. Alternatively, a large negative correlation between latent heat flux and SST tendency may indicate that the SST is forcing the atmosphere. It should be mentioned that this method of diagnosis is applicable only to local air–sea interactions and cannot account for remote teleconnections or the phase-shift relationship between the atmospheric variables and SST. Furthermore, Wu et al. (2006) used a simple stochastic model to show that such an analysis of atmospheric fluxes with SST and SST

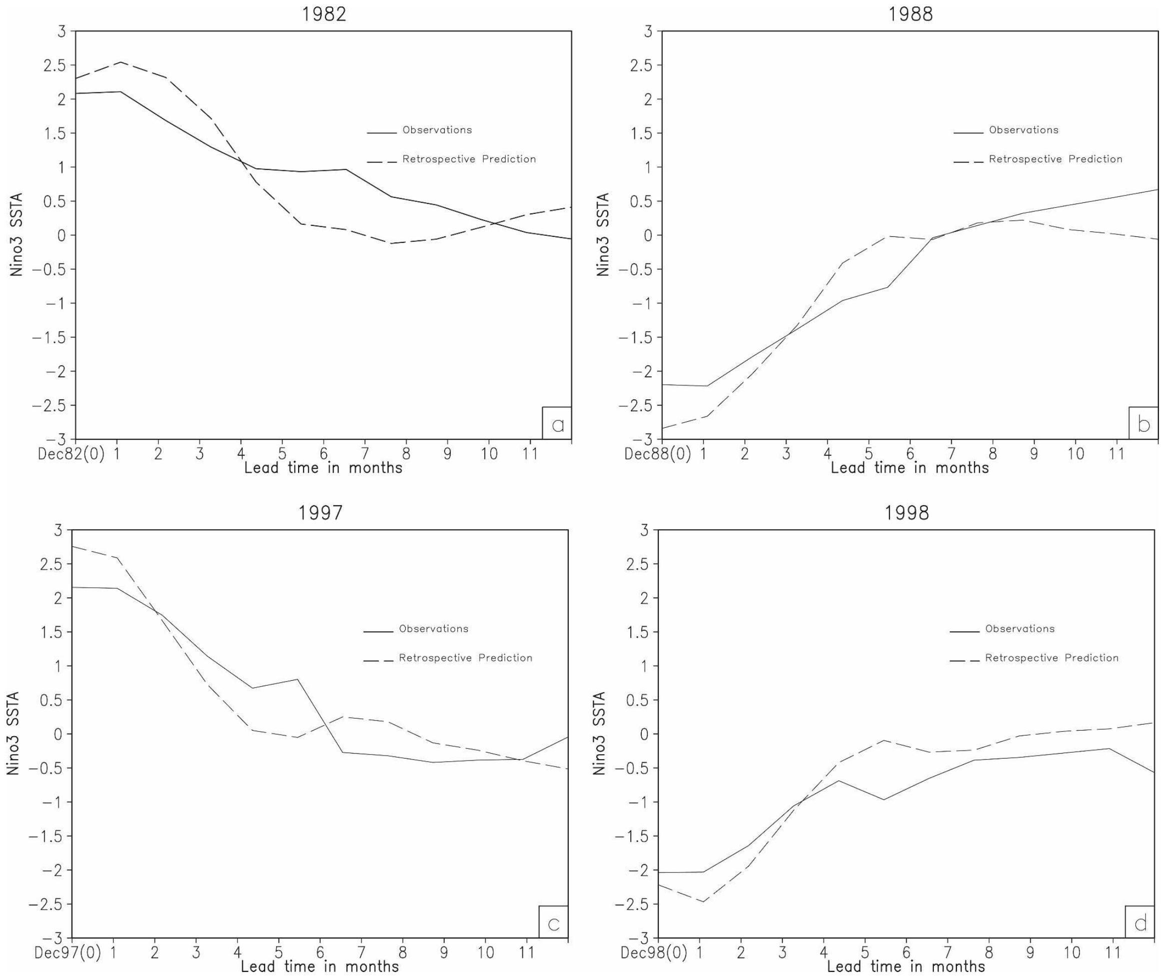

FIG. 4. The evolution of the Niño-3 SST anomalies from observations (ERSST2) and in the ensemble mean of the retrospective predictions in (a) 1982–83, (b) 1988–89, (c) 1997–98, and (d) 1998–99. The observed anomalies are computed with respect to the mean of the 4 yr shown.

tendencies is not overly sensitive to the use of monthly means instead of daily means.

In Figs. 5a–c we show the simultaneous correlation of latent heat flux with SST from observations, retrospective predictions, and simulation, respectively. The observed correlations in Fig. 5a were computed over a 13-yr period from January 1988 to November 2000. The observations indicate a strong positive correlation in the far eastern equatorial Pacific Ocean, with equally strong negative correlations in the western Pacific Ocean in either hemisphere, straddling the equator. In the retrospective predictions and in the simulation, the positive correlations over the equatorial Pacific extend erroneously too far to the west. In the simulation, the negative correlations over the western Pacific Ocean are weaker than the retrospective predictions and observations.

Similarly, the contemporaneous correlations of SST tendency with latent heat flux are shown in Figs. 5d–f. The simulation and retrospective predictions show very different features of air–sea interaction. Most importantly, it is apparent from weak correlations in the retrospective predictions (Fig. 5e)—contrary to either the simulation (Fig. 5f) or the observations (Fig. 5d)—that the atmosphere is not forcing the tropical and the subtropical Pacific Ocean. In the simulation, the negative correlations in the subtropical Pacific Ocean is erroneously strong. Furthermore, the large positive correlations in the far eastern equatorial Pacific Ocean are also contrary to the observations. However, the weaker correlations in the equatorial western Pacific Ocean in Fig. 5f match well with observations.

e. Differences in upper ocean variability

Zelle et al. (2004) in their observational study using subsurface ocean temperature measurements from

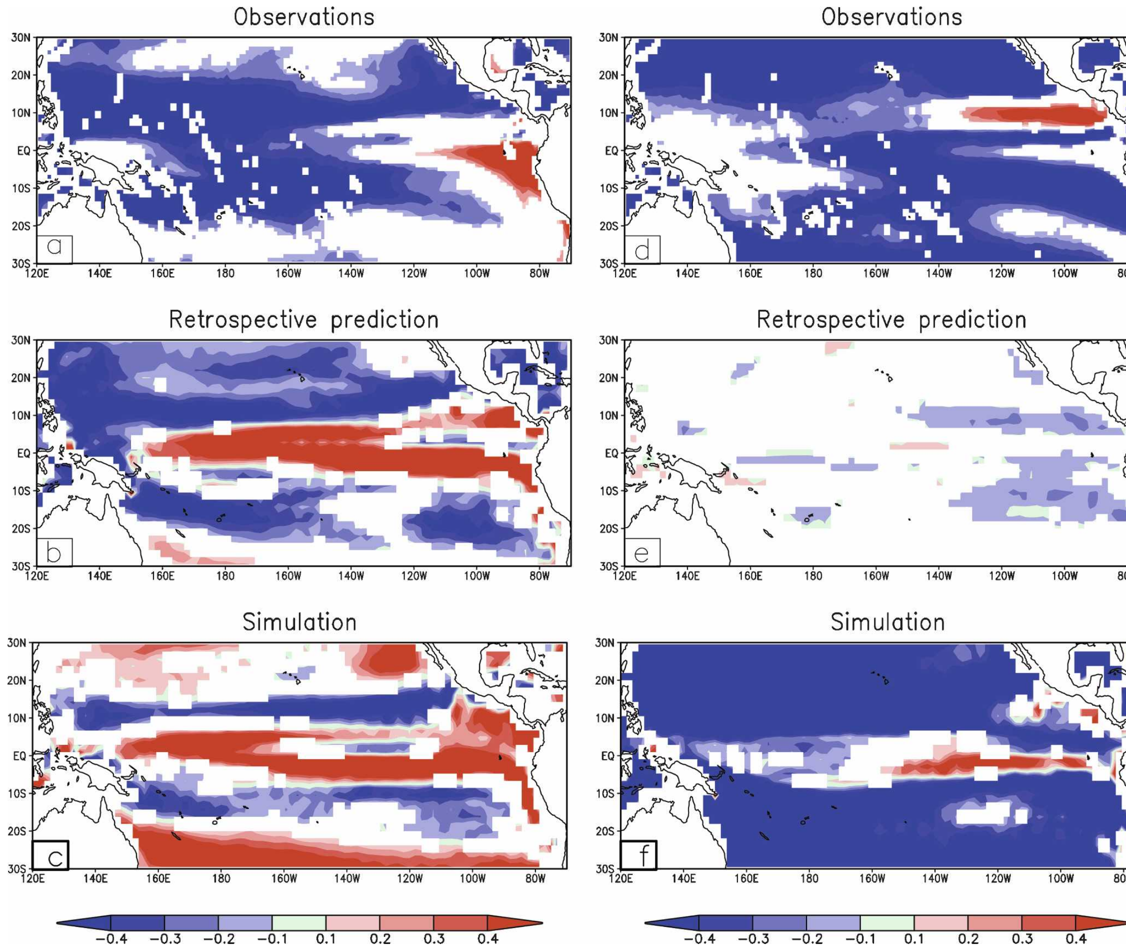

FIG. 5. Pointwise, contemporaneous correlation of evaporation with SST from (a) observations, (b) retrospective predictions, and (c) simulation. Similarly, pointwise, contemporaneous correlation of evaporation with SST tendency from (d) observations, (e) retrospective predictions, and (f) simulation. Significant values at 90% confidence interval according to a Student's *t* test are plotted.

Tropical Atmosphere Ocean Array–Triangle Trans-Ocean Buoy Network (TAO–TRITON) clearly showed significant correlations between thermocline depth and SST anomalies in excess of 0.9 over the eastern equatorial Pacific Ocean at different lead times. However, contemporaneous correlations in the far eastern equatorial Pacific between thermocline depth and SST were also significant (see their Fig. 2).

In Fig. 6 we have displayed a scatterplot, but between thermocline depth and SST over the Niño-3 region (150°–90°W, 5°S–5°N). The thermocline depth is diagnosed as the depth of the 20° isotherm. The observations in Fig. 6a refer to the ocean data assimilation of Rosati et al. (1997). The observations indicate a significant positive correlation between the two variables, consistent with the analysis of Zelle et al. (2004). In contrast, the retrospective predictions (Fig. 6b) show very little linear relationship between thermocline depth and SST, while the simulation results (Fig. 6c) are remarkably similar to the observations in Fig. 6a. This lack of linear relationship is also found at all lead times of the retrospective predictions (shown in Table 3).

The dynamical mechanism for this linear relationship between thermocline depth and SST in the Niño-3 region is a result of the strong upwelling (Zebiak and Cane 1987; Harrison and Vecchi 2001; Zelle et al. 2004). Using an OGCM and a simple linear model, Zelle et al. (2004) demonstrated that vertical advection of temperature anomalies from the thermocline to the surface and vertical mixing can produce the observed lag between the thermocline depth and SST, which ranges from 2 weeks to 2 months, between 90° and 140°W over the equator.

Following Kang et al. (2001) we have plotted in Figs. 7, 8 all the terms of the upper ocean (mixed layer) temperature anomaly equation (see the appendix) averaged in the upper 50 m of the ocean for both the retrospective predictions and the simulation. It should

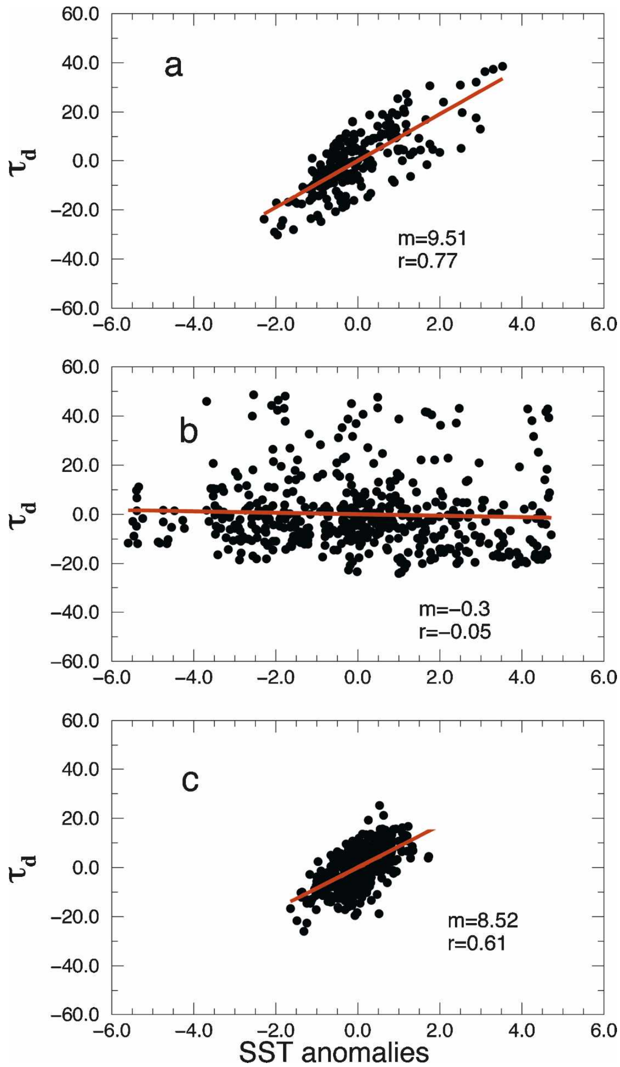

FIG. 6. Scatterplot of the anomalies of thermocline depth (m) vs SST anomalies (°C) over the Niño-3 region (150°–90°W, 5°S–5°N) from (a) observations, (b) retrospective predictions, and (c) simulation. The slope (*m*) and correlation (*r*) of the linear fit to the scatter are indicated in the legend.

TABLE 3. The slope and correlation (in brackets) of the linear relationship between thermocline depth and SST over the Niño-3 region as a function of time (lead time for retrospective prediction is indicated in brackets, while Julian month is shown for observations and the simulation).

Month	Observations	Retrospective prediction	Simulation
December (0)	9.22 (0.8)	−0.76 (−0.1)	6.82 (0.6)
January (l)	9.02 (0.7)	−0.28 (−0.1)	8.38 (0.7)
February (2)	8.3 (0.6)	0.85 (0.1)	9.5 (0.7)
March (3)	7.6 (0.5)	0.90 (0.1)	9.9 (0.8)
April (4)	9.55 (0.7)	−0.92 (−0.1)	8.3 (0.8)
May (5)	9.26 (0.76)	−6.97 (−0.4)	7.3 (0.5)
June (6)	8.46 (0.8)	−5.09 (−0.2)	12.39 (0.4)
July (7)	8.26 (0.8)	5.55 (−0.2)	6.54 (0.3)
August (8)	8.78 (0.9)	0.73 (0.0)	7.68 (0.4)
September (9)	10.05 (0.9)	4.66 (0.2)	9.71 (0.7)
October (10)	11.72 (0.9)	5.24 (0.2)	9.2 (0.8)
November (ll)	10.82 (0.9)	1.82 (0.1)	6.8 (0.6)

be noted that in these figures, unlike in Kang et al. (2001), the covariance of the advection terms with the Niño-3 SST index tendency (calculated from the monthly mean values) is shown at zero lag divided by the standard deviation of the Niño-3 SST index tendency. These covariances provide the actual magnitude of the advection term related to the Niño-3 SST index. The diffusion term is relatively small. Furthermore, it is uncorrelated to Niño-3 SST index tendency and therefore is not shown in Figs. 7, 8.

A striking difference between the retrospective predictions and the simulation is that in the former the advection terms related to the horizontal currents (both mean and the anomalous) are contributing relatively more to the Niño-3 SST variability (Figs. 7a–d) than in the latter (Figs. 8a–d). This intense activity of the horizontal advection terms seems to contribute to the changes in the thermocline–SST, atmophere fluxes–SST, and SST tendency relationships, despite comparable advection of both the mean and the anomalous upwelling in the retrospective predictions (Figs. 7e,f) and in the simulation Figs. 8e,f).

5. Discussion and conclusions

In summary, we have shown that differences exist in the mean state and in the variability of the tropical Pacific between retrospective seasonal predictions and a multidecadal integration of the same coupled climate model. These differences manifest in magnitude of the model bias and variability of the SST, as well as in the nature of the air–sea coupled interactions and in the upper ocean variability. Because identical models were used, these differences could be attributed to initialization errors. It can be argued that these differences may also be a result of choosing big ENSO events in the retrospective prediction cases, while the multidecadal simulation includes a relatively wider range of conditions in the equatorial Pacific. To alleviate this doubt, we recalculated the simulation results of this study by eliminating 12 neutral years of the 40 yr of the integration. The conclusions of the study remained unchanged.

It has to be mentioned that the mechanism of ENSO in the long-term integration of the COLA coupled model is consistent with the observed dominance of the vertical advection of the anomalous temperature by the mean upwelling in the equatorial Pacific and the merid-

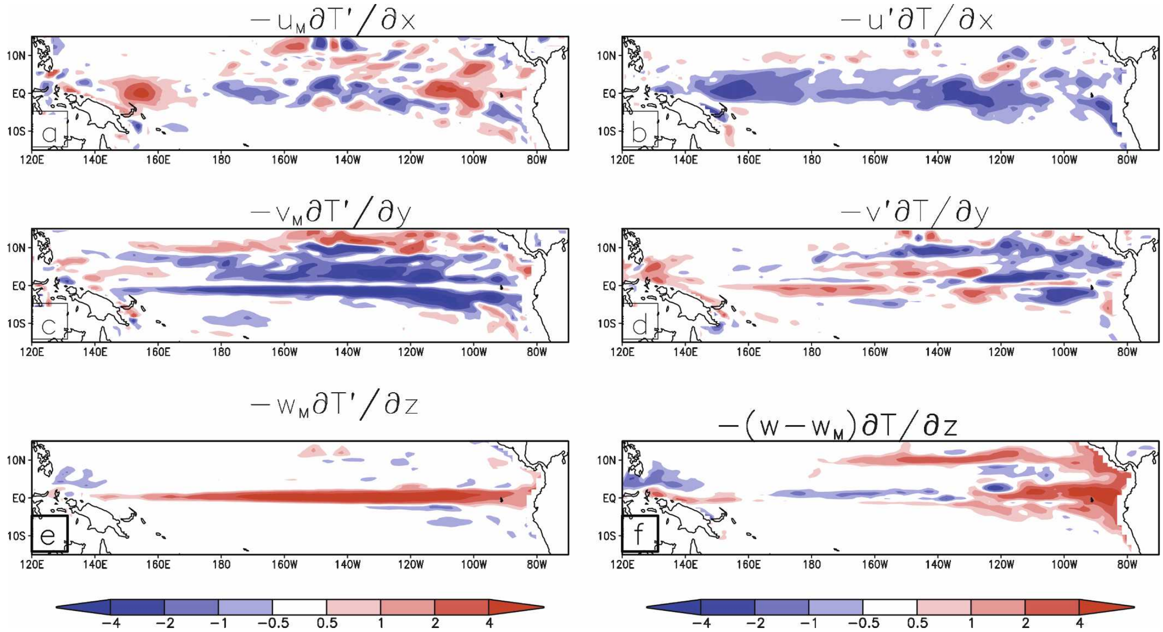

FIG. 7. The covariance of the Niño-3 SST index tendency with (a) term 1, (b) term 2, (c) term 3, (d) term 4, (e) term 5, and (f) term 6 of the right-hand side of the SST anomaly equation (see the appendix) divided by the std dev of the Niño-3 SST index tendency from the retrospective prediction runs. The units are nondimensional and scaled by 10^{-1}.

ional flux divergence by the mean meridional current, which drains the heat in the ocean surface from the equator into the off-equator (Kang et al. 2001). Consequently, the thermocline depth and SST relationship in the simulation is consistent with the observations.

However, it may be noted that the drift in the long-term simulations of the contemporary coupled climate models is also very significant (AchutaRao et al. 2004). It is found that all coupled models suffer with an equatorial cold tongue bias, erroneous split ITCZ phenomenon, lack of adequate stratus clouds in the eastern oceans, and concomittant inadequate upwelling along

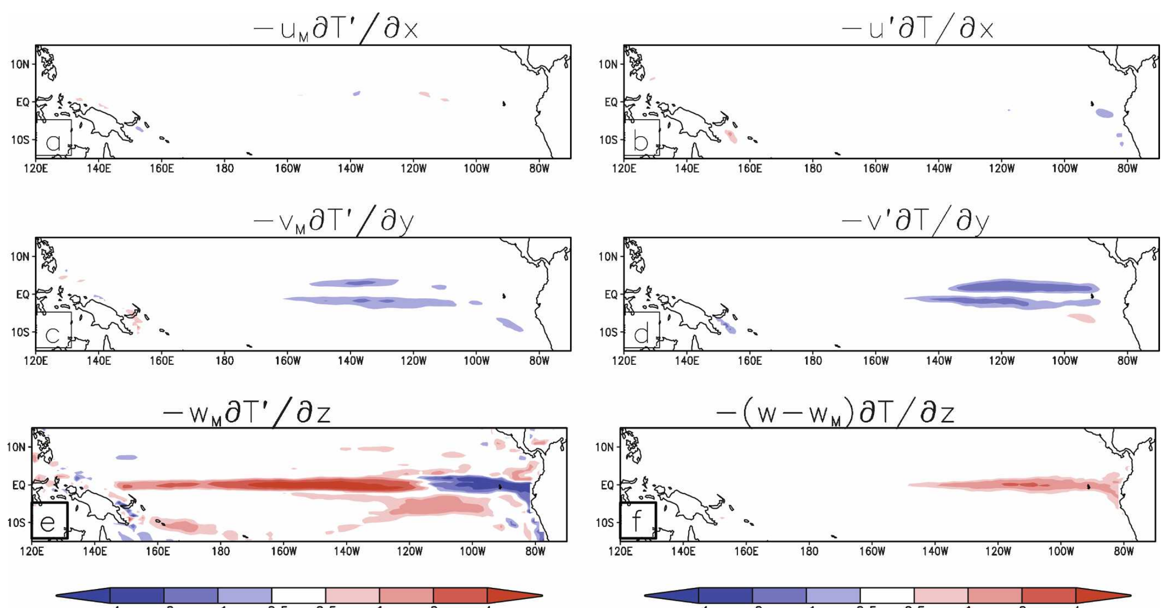

FIG. 8. Same as Fig. 7, but for the simulation.

the eastern boundary. Some of the common ENSO bias across these models included a narrow meridional extent, erroneous westward extension of the variability west of the date line, and periodicity and erroneous amplitude. The COLA coupled model is no exception to these issues (Misra et al. 2007).

We therefore argue that in an imperfect model (with relatively large errors) realistic ocean conditions produce imbalances that result in initialization shock when predictions are made with such a model. As a consequence, the model features as diagnosed from these predictions are different from those diagnosed from a long-term integration of the same model. This initialization shock may be of differing magnitude and may manifest itself in other ways in different coupled climate models. In this study, we have demonstrated that in the coupled COLA climate model, the air–sea interaction physics and upper ocean dynamics over the tropical Pacific Ocean are modified based on the mode of operation of the model. This paper highlights that initializing the coupled climate models is a daunting challenge to the climate prediction community.

Acknowledgments. This study was supported by NSF Grant ATM0332910, NASA Grant NNG04GG46G, and NOAA Grant NA04OAR4310034. We also acknowledge the use of computing resources at the NASA Ames facility under NASA Project NNG06GB54G and Columbia Project SMD-05-0115.

APPENDIX

Upper Ocean Temperature Anomaly Equation

The upper ocean temperature anomaly equation, following Kang et al. (2001), is

$$\frac{\partial T'}{\partial t} = -u_M\frac{\partial T'}{\partial x} - u'\frac{\partial T}{\partial x} - v_M\frac{\partial T'}{\partial y} - v'\frac{\partial T}{\partial y} - w_M\frac{\partial T'}{\partial z} - (w - w_M)\frac{\partial T}{\partial z} - Q'. \tag{1}$$

In Eq. (1), the $'$ denotes deviation from the time mean. The first term on the right-hand side of Eq. (1) (term 1) is the advection by the mean zonal current of the anomalous temperature. The second term (term 2) is the advection of the total temperature by the anomalous zonal current. Likewise, terms 3 and 4 are the corresponding meridional components of advections. Term 5 corresponds to vertical advection of the anomalous temperature by the mean vertical velocity. Term 6 refers to the vertical advection of the total temperature by the anomalous vertical velocity. The last term (Q') includes the anomalous heat flux, diffusion, and vertical mixing. In plotting Figs. 7, 8 we have averaged the right-hand-side terms in the upper 50 m to represent the mixed layer of the ocean.

REFERENCES

AchutaRao, K., C. Covey, C. Doutriaux, M. Fiornio, P. Gleckler, T. Phillips, K. Sperber, and K. Taylor, 2004: An appraisal of coupled climate model simulations. Lawrence Livermore National Laboratory Rep. UCRL-TR-202550, 197 pp. [Available online at http://www-pcmdi.llnl.gov/model_appraisal.pdf.]

Bacmeister, J., and Coauthors, 2000: An atlas of seasonal means simulated by the NSIPP-1 atmospheric GCM. NASA Goddard Space Flight Center Tech. Memo. 104606, 17, 194 pp.

Briegleb, B. P., 1992: Delta-Eddington approximation for solar radiation in the NCAR community climate model. *J. Geophys. Res.,* **97,** 7603–7612.

Cayan, D. R., 1992: Latent and sensible hat flux anomalies over the northern oceans: Driving the sea surface temperature. *J. Phys. Oceanogr.,* **22,** 859–881.

Chou, S.-H., E. Nelkin, J. Ardizzone, R. M. Atlas, and C.-L. Shie, 2003: Surface turbulent heat and momentum fluxes over global oceans based on Goddard satellite retrievals, version 2(GSSTF2). *J. Climate,* **16,** 3256–3273.

Collins, W. D., J. K. Hackney, and D. P. Edwards, 2002: An updated parameterization for infrared emission and absorption by water vapor in the National Center for Atmospheric Research Community Atmosphere Model. *J. Geophys. Res.,* **107,** 4664, doi:10.1029/2001JD001365.

Dirmeyer, P. A., and F. J. Zeng, 1999: Precipitation infiltration in the simplified SiB land surface scheme. *J. Meteor. Soc. Japan,* **78,** 291–303.

——, and L. Tan, 2001: A multi-decadal global land-surface data set of state variables and fluxes. COLA Tech. Rep. 102, 46 pp. [Available online at http://grads.iges.org/pubs/ctr_102.pdf.]

Harrison, D., and G. A. Vecchi, 2001: El Niño and La Niña—Equatorial Pacific thermocline depth and sea surface temperature anomalies, 1986–98. *Geophys. Res. Lett.,* **28,** 1051–1054.

Hong, S. Y., and H.-L. Pan, 1996: Nonlocal boundary layer vertical diffusion in a medium-range forecast model. *Mon. Wea. Rev.,* **124,** 2322–2339.

Jin, E. K., and Coauthors, 2008: Current status of ENSO prediction skill in coupled ocean–atmosphere models. *Climate Dyn.,* doi: 10.1007/s00382-008-0397-3.

Kalnay, E., and Coauthors, 1996: The NCEP/NCAR 40-Year Reanalysis Project. *Bull. Amer. Meteor. Soc.,* **77,** 437–471.

Kang, I.-S., I.-S. An, and F.-F. Jin, 2001: A systematic approximation of the SST anomaly equation for ENSO. *J. Meteor. Soc. Japan,* **79,** 1–10.

Kiehl, J. T., J. J. Hack, G. Bonan, B. A. Boville, D. L. Williamson, and P. J. Rasch, 1998: The National Center for Atmospheric Research Community Climate Model: CCM3. *J. Climate,* **11,** 1131–1149.

Kirtman, B. P., D. A. Paolino, J. L. Kinter III, and D. M. Straus, 2001: Impact of tropical subseasonal SST variability on seasonal mean climate simulations. *Mon. Wea. Rev.,* **129,** 853–868.

Latif, M., and Coauthors, 1998: A review of the predictability and prediction of ENSO. *J. Geophys. Res.,* **103,** 14 375–14 393.

Misra, V., 2004: An evaluation of the predictability of austral summer season precipitation over South America. *J. Climate,* **17,** 1161–1175.

——, and Coauthors, 2007: Validating and understanding ENSO simulation in two coupled climate models. *Tellus,* **59A,** 292–308.

Pacanowski, R. C., and S. M. Griffies, 1998: MOM3.0 manual. NOAA/Geophysical Fluid Dynamics Laboratory, Princeton, New Jersey, 561 pp.

Philander, S. G. H., 1983: El Niño–Southern Oscillation phenomena. *Nature,* **302,** 295–301.

Rosati, A., R. Gudgel, and K. Miyakoda, 1997: The impact of ocean initial conditions on ENSO forecasting with a coupled model. *Mon. Wea. Rev.,* **125,** 754–772.

Saha, S., and Coauthors, 2006: The NCEP Climate Forecast System. *J. Climate,* **19,** 3483–3517.

Smith, T. M., and R. W. Reynolds, 2003: Extended reconstruction of global sea surface temperatures based on COADS data (1854–1997). *J. Climate,* **16,** 1495–1510.

Tiedtke, M., 1984: The effect of penetrative cumulus convection on the large-scale flow in a general circulation model. *Beitr. Phys. Atmos.,* **57,** 216–239.

Wallace, J. M., C. Smith, and Q.-R. Jiang, 1990: Spatial patterns of atmosphere–ocean interaction in the northern winter. *J. Climate,* **3,** 990–998.

Wu, R., B. P. Kirtman, and K. Pegion, 2006: Local air–sea relationship in observations and model simulations. *J. Climate,* **19,** 4914–4932.

Xue, Y.-K., P. J. Sellers, J. L. Kinter, and J. Shukla, 1991: A simplified biosphere model for global climate studies. *J. Climate,* **4,** 345–364.

——, F. J. Zeng, and C. A. Schlosser, 1996: SSiB and its sensitivity to soil properties. A case study using HAPEX-Mobilhy data. *Global Planet. Change,* **13,** 183–194.

Zebiak, S. E., and M. A. Cane, 1987: A model El Niño–Southern Oscillation. *Mon. Wea. Rev.,* **115,** 2262–2278.

Zelle, H., G. Appeldoorn, G. Burgers, and G. J. van Oldenborgh, 2004: The relationship between sea surface temperature and thermocline depth in the eastern equatorial Pacific. *J. Phys. Oceanogr.,* **34,** 643–655.